Transport and loss of the inner plasma sheet electrons: THEMIS observations

S. Kurita,[1] Y. Miyoshi,[2] F. Tsuchiya,[1] Y. Nishimura,[2,3] T. Hori,[2] Y. Miyashita,[2] T. Takada,[4] A. Morioka,[1] V. Angelopoulos,[5] J. P. McFadden,[6] H. U. Auster,[7] J. M. Albert,[8] V. Jordanova,[9] and H. Misawa[1]

Received 27 July 2010; revised 31 October 2010; accepted 27 December 2010; published 1 March 2011.

[1] Using the electron data from the Time History of Events and Macroscale Interactions during Substorms (THEMIS) spacecraft measurements from 2007 to 2009, we derived global phase space density (PSD) distributions of plasma sheet electrons (2–100 eV/nT) to examine the transport process of the electrons to the inner magnetosphere and possible loss mechanisms of plasma sheet electrons during the convective transport. The inner boundaries of the electron plasma sheet were determined by the observed global distributions and compared with the Alfvén boundaries that were calculated by the sum of the simple corotation and convection electric field models. This comparison confirms the previous results that the large-scale convection electric field controls the electron transport to the inner magnetosphere. The gradual decrease in PSD is observed from the dawn to the dayside sector, indicating the existence of some loss mechanisms in the morning sector. The loss time scales estimated from the PSD distributions were compared with the theoretical ones based on the quasi-linear diffusion theory using an empirical wave model of whistler mode chorus. We also estimated the required wave amplitudes that can explain the estimated loss time scales. It is shown that whistler mode chorus has a sufficient power to scatter the plasma sheet electrons, and the required wave amplitudes are roughly consistent with the CRRES statistical survey of the chorus wave amplitude. We suggest that the loss of plasma sheet electrons in the morning sector is mainly induced by pitch angle scattering by whistler mode chorus.

Citation: Kurita, S., et al. (2011), Transport and loss of the inner plasma sheet electrons: THEMIS observations, *J. Geophys. Res.*, *116*, A03201, doi:10.1029/2010JA015975.

1. Introduction

[2] The plasma sheet is the primary reservoir of hot plasma in the magnetosphere and is believed to be the source of the energetic particles injected into the inner magnetosphere during substorms and storms [e.g., *Kerns et al.*, 1994; *Birn et al.*, 1997]. It is thought that the injected energetic ions contribute to the evolution of the ring current population, and many ring current simulations have used the plasma sheet properties as boundary conditions for the calculations [e.g., *Jordanova et al.*, 1998, 2006; *Ebihara et al.*, 2002]. The energetic electrons of the plasma sheet are also important because they play a significant role in the seed population of relativistic electrons in the radiation belts [e.g., *Miyoshi et al.*, 2003, 2007]. A recent study by *Wang et al.* [2008] clearly showed, based on a case study, that plasma sheet particles penetrate earthward into the inner magnetosphere during the storm main phase and that plasma sheet particles are adiabatically energized to tens of keV to a few hundred of keV, resulting in an increase in the population of energetic particles in the inner magnetosphere. The result emphasizes the importance of the plasma sheet conditions to the configuration of the particle distribution in the inner magnetosphere.

[3] *Korth et al.* [1999] statistically examined the plasma environment at geosynchronous orbit sorted by the *Kp* index using the LANL MPA data, and they applied the particle drift paradigm to their observations. The results showed that a simple *Kp*-dependent convection electric field model,

[1]Planetary Plasma and Atmospheric Research Center, Tohoku University, Sendai, Japan.
[2]Solar-Terrestrial Environment Laboratory, Nagoya University, Nagoya, Japan.
[3]Also at Department of Atmospheric and Oceanic Sciences, University of California, Los Angeles, California, USA.
[4]Department of Electrical Engineering and Information Science, Kochi National College of Technology, Nankoku, Japan.
[5]Institute of Geophysics and Planetary Physics, University of California, Los Angeles, California, USA.
[6]Space Sciences Laboratory, University of California, Berkeley, California, USA.
[7]Institut für Geophysik und Extraterrestrische Physik, Technische Universität Braunschweig, Braunschweig, Germany.
[8]Space Vehicles Directorate, Air Force Research Laboratory, Hanscom Air Force Base, Massachusetts, USA.
[9]Los Alamos National Laboratory, Los Alamos, New Mexico, USA.

0148-0227/11/2010JA015975

together with the concept of the Alfvén boundaries, successfully ordered their data and demonstrated the average plasma sheet access to geosynchronous orbit during both quiet and disturbed times. *Friedel et al.* [2001] extended the work by *Korth et al.* [1999] to cover the inner magnetosphere by using data obtained from the Polar HYDRA instrument. The results showed good agreement between the averaged inner boundaries from the data and the predicted boundaries in a global sense. These studies also pointed out that the electron flux on the dayside is depleted compared with that on the nightside, and suggested that electrons precipitate into the atmosphere through wave-particle interactions during the convective transport from the nightside to the dayside. However, there were no discussions about the wave mode that mainly contributes to the scattering of plasma sheet electrons, and no quantitative analyses of the electron losses.

[4] It has been believed that the central plasma sheet is the source region of the particles for diffuse auroras [*Lui et al.*, 1977; *Meng et al.*, 1979] and the diffuse aurora is believed to be the result of pitch angle scattering of plasma sheet electrons into the loss cone by wave-particle interactions [*Fontaine and Blanc*, 1983]. Thus, the wave-particle interactions are an important loss mechanism of the plasma sheet electrons. Both electron cyclotron harmonic (ECH) waves and the whistler mode chorus resonate with the plasma sheet electrons [*Horne et al.*, 2003a], and the main contributor of the diffuse aurora (i.e., sweeper of the plasma sheet electrons) has been discussed by many researchers, but it is still a subject of controversy in magnetospheric physics [e.g., *Belmont et al.*, 1983; *Roeder and Koons*, 1989; *Horne and Thorne*, 2000; *Ni et al.*, 2008].

[5] The wave modes that contribute the loss of plasma sheet electrons have been discussed mainly based on wave observations and calculations of the pitch angle diffusion rates. In the 1970s, the calculations of pitch angle scattering rate [*Lyons*,1974] based on the initial OGO-5 wave observations [*Kennel et al.*, 1970] indicated that the amplitudes of ECH waves are large enough to scatter the electrons with energies from a few hundred eV to several keV, suggesting that the ECH waves are responsible for the loss of the plasma sheet electrons. However, in the 1980s, statistical surveys of occurrence rate of ECH waves indicated that the amplitude of ECH waves rarely have the sufficient power to scatter the plasma sheet electrons [e.g., *Belmont et al.*, 1983; *Roeder and Koons*, 1989]. The new calculation of pitch angle diffusion done by *Horne and Thorne* [2000] suggested that the ECH waves can scatter the plasma sheet electrons when the waves lie the favored frequency ranges. Recently, *Ni et al.* [2008] calculated the pitch angle diffusion rate by whistler mode chorus during active conditions on the nightside. The result showed that the rate of pitch angle scattering exceed the strong diffusion rate over a broad energy range below a few keV and is greater than the scattering rate by the ECH waves. Their result suggested that the whistler mode chorus can also play a major role in the loss of the plasma sheet electrons during active conditions.

[6] The loss time scale of radiation belt electrons have been investigated by particle measurements and quantitatively compared them with the theoretical loss time scale based on the pitch angle diffusion rate [e.g., *Lyons et al.*, 1972; *Meredith et al.*, 2009]. Therefore, it is possible to identify the wave modes that contribute the loss of radiation belt electrons, and it seems that this method would be useful for the estimation of loss processes of plasma sheet electrons. However, to our knowledge, there have been no estimations and detailed discussions of the loss time scales of plasma sheet electrons based on electron measurements.

[7] In the present study, we establish the two objectives and clarify them by using the global electron distributions based on the Time History of Events and Macroscale Interactions during Substorms (THEMIS) observations. The first objective is to examine the transport process of plasma sheet electrons to the inner magnetosphere and its dependence on geomagnetic activities. We also compare the averaged distributions derived from the THEMIS observations with the calculations based on convective transport in the inner magnetosphere. The second objective is to quantitatively estimate the loss time scales of plasma sheet electrons during convective transport using the global electron distributions, which is the primary target of the present study. Note that qualitative discussions about the loss mechanisms of the plasma sheet electrons have given by the previous observational studies [*Korth et al.*, 1999; *Friedel et al.*, 2001]. The recent data from the THEMIS satellites were used for the analysis because the five spacecraft can provide us much higher spatial resolution data and sufficiently cover the inner magnetospheric regions near the equatorial plane. Using the data obtained by THEMIS, we show electron distributions in the inner magnetosphere and the global view of the inner boundaries of the electron plasma sheet. Furthermore, we estimate the loss time scales based on the electron measurements for the first time, and discuss possible loss processes of plasma sheet electrons on the morning side in the inner magnetosphere.

2. Instruments and Data Analysis

[8] The THEMIS mission consists of five identical spacecraft placed near the magnetic equator with perigees below 2 R_E and apogees above 10 R_E, and the apogees slowly rotate around the Earth [*Angelopoulos*, 2008]. The THEMIS satellite data enable analyzing statistically the spatial distributions of electrons in the region where the previous missions were not able to cover sufficiently. In this study, we use electron data obtained by the electrostatic analyzer (ESA, 7 eV to 26 keV for electrons) [*McFadden et al.*, 2008a] and magnetic field data obtained by the fluxgate magnetometer (FGM) [*Auster et al.*, 2008]. Omnidirectional electron energy fluxes and magnetic field data are included in the survey mode telemetry, covering most orbits with a measurement cadence of ~3 s. The analysis period in this study is from August 2007 to August 2009. Because there were no major storms with a Dst index of less than −100 nT during the analysis period, the electron distributions during quiet and moderately disturbed conditions can be obtained in this study.

[9] To determine the global distributions of plasma sheet electrons, we use the phase space density (PSD) as a function of the first adiabatic invariant, which is suitable for studying adiabatic transport. We select the values of the first

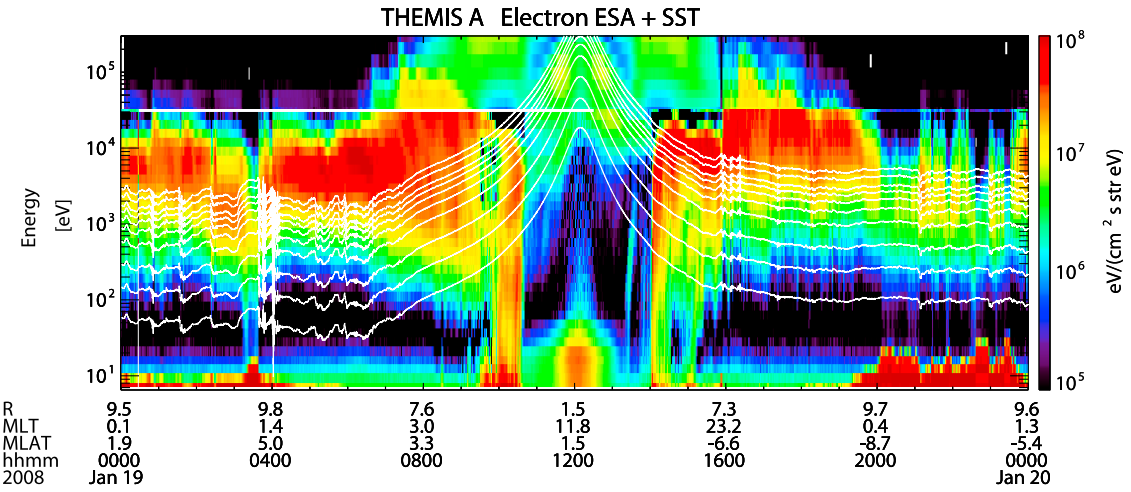

Figure 1. Energy-time spectrogram after the background subtraction measured by THEMIS-A. White lines indicate variations of the energies corresponding to several first adiabatic invariants. The first adiabatic invariants are derived from the in situ magnetic field measured by FGM. Ten traces correspond to 2.0, 5.0, 10, 20, 30, 40, 50, 60, 80, and 100 eV/nT.

adiabatic invariants: 2.0, 5.0, 10, 20, 30, 40, 50, 60, 80, and 100 eV/nT. The first adiabatic invariant μ is given by

$$\mu = \frac{p_\perp^2}{2m_0 B}, \tag{1}$$

where $p_\perp$ is the relativistic momentum of a particle perpendicular to the ambient magnetic field, m_0 is the electron rest mass, and B is the ambient magnetic field intensity. The statistical distribution of the PSD in the equatorial plane for each first adiabatic invariant is evaluated in the following way: We divided a region of $-15 \le X \le 15\ R_E$ and $-15 \le Y \le 15\ R_E$ into bins with a size of $0.5\ R_E \times 0.5\ R_E$ in solar magnetic (SM) coordinates. The PSD (in units of $eV^{-3}\ s^{-3}$) for each first adiabatic invariant was calculated, assuming that electrons with a local pitch angle of 90° are dominant at the spacecraft locations close to the magnetic equator. Then, the averaged PSD in each bin was evaluated. The local spacecraft positions (X_{SM}, Y_{SM}) were used to calculate the average PSD. The position of the magnetopause was determined by the Tsyganenko 89c *Kp*-dependent magnetic field model[*Tsyganenko*, 1989]. The data outside of the magnetosphere were excluded from the analysis.

[10] Since it is essential to minimize uncertainty due to the off equatorial measurements, we only used the data obtained in a magnetic latitude range of −10 to 10°. In this magnetic latitude range, the discrepancy between the local spacecraft position and the location of the magnetic equator along the Tsyganenko 89c magnetic field models is generally less than $0.5\ R_E$. Also, we have examined the uncertainty of the fluxes due to the measurements at different magnetic latitudes referring the averaged anisotropy of electrons shown by *Li et al.* [2010]. The examination indicates that the data acquired in the magnetic latitude range of −10 to 10° would be enough for the discussions in this study because we are interested in the PSD variations with more than an order of magnitude and the flux variation along the mapping is only less than a factor of 2.

[11] While THEMIS covers the whole region of the inner magnetosphere, the particle data for the inner magnetosphere are generally contaminated by radiation belt particles. In this study, we have used an automated noise correction, which subtracted the high-energy particle noise component from the original data given as the count rate [*McFadden et al.*, 2008b]. This method is similar to the one used for the FAST particle data [*Yao et al.*, 2008], where they subtracted the high-energy electron noise from the original data using the count rate in the loss cone. Since THEMIS/ESA cannot observe the exact count rate within the loss cone because the local loss cone near the equatorial region is much smaller than the angular size of the ESA instrument, we define the background level as the smallest omnidirectional count rate in the ESA energy channel at one time and subtract it from the original omnidirectional data.

[12] The energy flux spectrogram combined with ESA and Solid State Telescope (SST, ~28 keV to ~1 MeV for electrons) [*Angelopoulos*, 2008] of THEMIS-A is shown in Figure 1. The white curves indicate the electron energy for each first adiabatic invariant calculated from the in situ magnetic field data. The population of plasma sheet electrons is in the high-flux region ($\gtrsim 10^6$ eV/(cm^2 s str eV)) with an energy of several hundred eV to ~20 keV in the spectra. The selected first invariants correspond to the low-energy component of the electron plasma sheet. The spectrogram in Figure 1 indicates that the background subtraction is successful and enables us to discriminate the inner edge of the electron plasma sheet even under the severe contamination of the radiation belt particles (not shown).

[13] The Alfvén boundary of electrons with each first adiabatic invariant is calculated and overplotted onto the averaged data to compare the observations with the theoretical estimation of the electron access. The calculations of Alfvén boundary position is based on the (U, B, K) formulation introduced by *Whipple* [1978], and this framework for analysis of particle trajectories has also used by *Korth et al.* [1999] and *Friedel et al.* [2001]. The (U, B, K) formulation

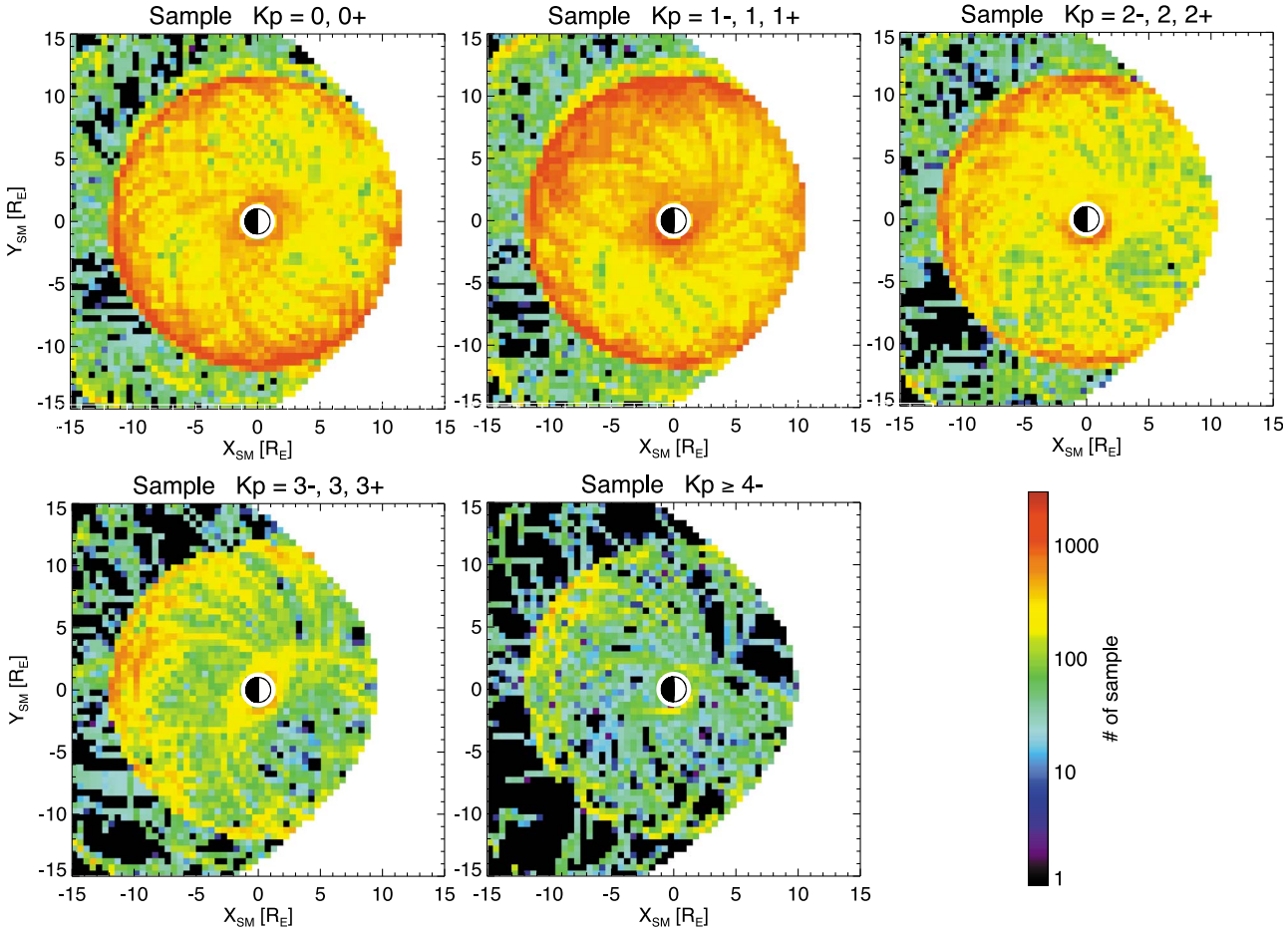

Figure 2. Spatial distribution of the number of data in each bin used for the statistical analysis.

defines a particle total energy using the electric potential and magnetic field intensity:

$$W = qU + \mu B_m, \tag{2}$$

where q is the particle charge, U is the electric potential, and B_m is the magnetic field intensity at the mirror point. The quantity K is proportional to the second adiabatic invariant J, but, assuming an equatorial pitch angle of 90° in this study, the K coordinate can be omitted and B_m can be replaced by the equatorial magnetic field intensity. In the coordinate system, all particle trajectories become straight lines with slopes proportional to the particle's first adiabatic invariant:

$$\frac{\partial U}{\partial B} = -\frac{\mu}{q}. \tag{3}$$

All boundaries are calculated by using the dipole magnetic field model and superposition of shielded dawn-dusk electric field with a corotation electric field, which is often called the Volland-Stern electric field model [*Volland*, 1973; *Stern*, 1975]:

$$U = -\frac{a}{r} - br^{\gamma}\sin(\phi), \tag{4}$$

where r is the radial distance from the center of the Earth, ϕ is the magnetic local time referred to from noon, γ is the shielding factor, and a = 92.4kV R_E^{-1} is the corotation constant. The convection electric field component b has been parameterized by the geomagnetic activity level as indicated by the Kp index for a shielding factor of $\gamma = 2$ [*Maynard and Chen*, 1975]. The dependence is expressed as:

$$b = \frac{0.045}{(1 - 0.159Kp + 0.0093Kp^2)^3}, \tag{5}$$

where the unit is kV R_E^{-1}. For the case of $Kp \geq 4-$, we fix the value of the Kp index to 4.

3. Observations

3.1. Electron Transport Into the Inner Magnetosphere

[14] Figure 2 shows the data coverage in the $X_{SM} - Y_{SM}$ plane for the analysis period. The electron data are sorted by geomagnetic activity into five Kp index ranges: 0 to 0+, 1− to 1+, 2− to 2+, 3− to 3+, and ≥ 4−. The color intensity scale represents the number of samples in each bin from 1 to 3000. As shown in Figure 2, the number of samples generally exceeds 50 for all cases and it exceeds 150 especially below 10 R_E except for $Kp \geq 4-$. Since the Alfvén boundary

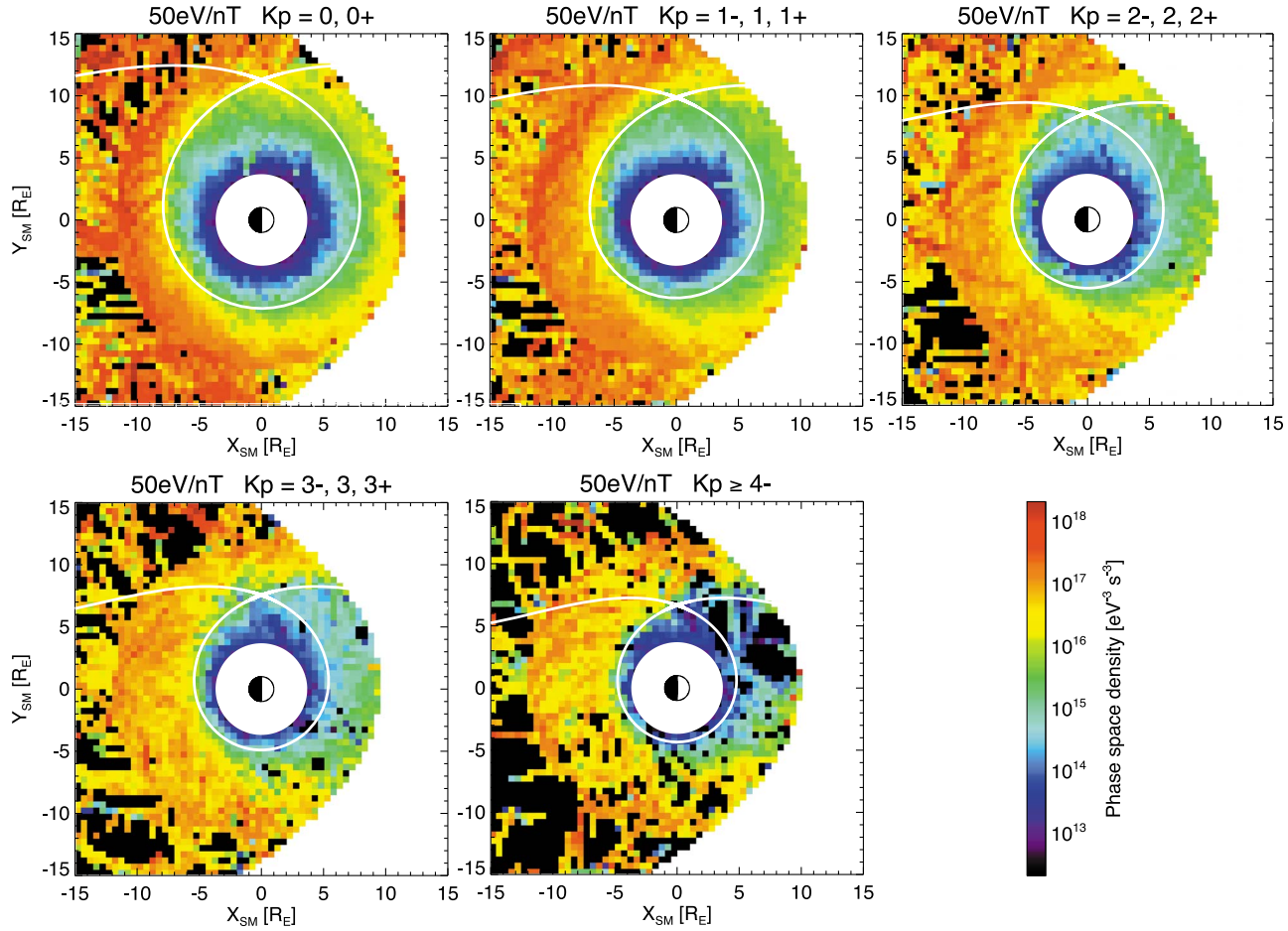

Figure 3. Average distributions of the phase space density of electrons with 50 eV/nT. White circle near the Earth is the region where electron energy exceeds limit of measurement of ESA. The calculated Alfvén boundary is overplotted by a white line.

generally exists below 10 R_E for the first adiabatic invariant range considered here, the *Kp* dependence of the Alfvén boundary can be reliably investigated based on a larger number of samples. The number of samples is relatively low above 10 R_E, so the electron distribution outside 10 R_E is not discussed in this paper.

[15] Figures 3 and 4 show electron PSDs for μ = 50 and 100 eV/nT, respectively. It is expected that the electron flux is significantly small inside the Alfvén boundary, so that the region between low flux on the earthward side and high flux should be correspond to the Alfvén boundary. Figures 3 and 4 show that the observed boundary position depends on the magnetic local time (MLT) and that the position closely follows the Alfvén boundary shown by the white curves.

[16] A first adiabatic invariant of 50 eV/nT (Figure 3) corresponds to ~7 keV at geosynchronous orbit. A good agreement between the observed boundary position and the calculated Alfvén boundary can be clearly found from ~18 to ~4 MLT through the midnight sector. From ~04 to ~18 MLT through the dayside sector, the PSD decreases as the electrons drift from the dawnside to the dayside sectors. Since electrons spend a long time drifting from the magnetotail to the dayside magnetopause, it is expected that some of the electrons precipitate into the atmosphere by the pitch angle scattering through wave-particle interactions [e.g., *Thomsen et al.*, 1998]. Even though the gradient of the PSD may not be as sharp as on the nightside because of some loss processes of electrons, the calculated Alfvén boundary still follows the color contour of the PSD. As *Kp* increases, the calculated Alfvén boundaries shrink, and good agreements can be still found between the boundary positions and the calculations although the gradients of the PSD in the dayside are not sharper than the nightside as also seen at the low *Kp*. At *Kp* = 0, the calculated Alfvén boundary is located near 8 and 10.5 R_E at midnight and dusk, respectively, while for $Kp \geq 4$, the calculated Alfvén boundary lies about 4.5 and 6 R_E at midnight and dusk, respectively.

[17] A first adiabatic invariant of 100 eV/nT for electrons (Figure 4) corresponds to ~14 keV at geosynchronous orbit. We can see the same MLT dependence identified in Figure 3. The only difference between μ = 50 and 100 eV/nT is the radial distance of both the boundary position and the calculated Alfvén boundary. The boundary position and the cal-

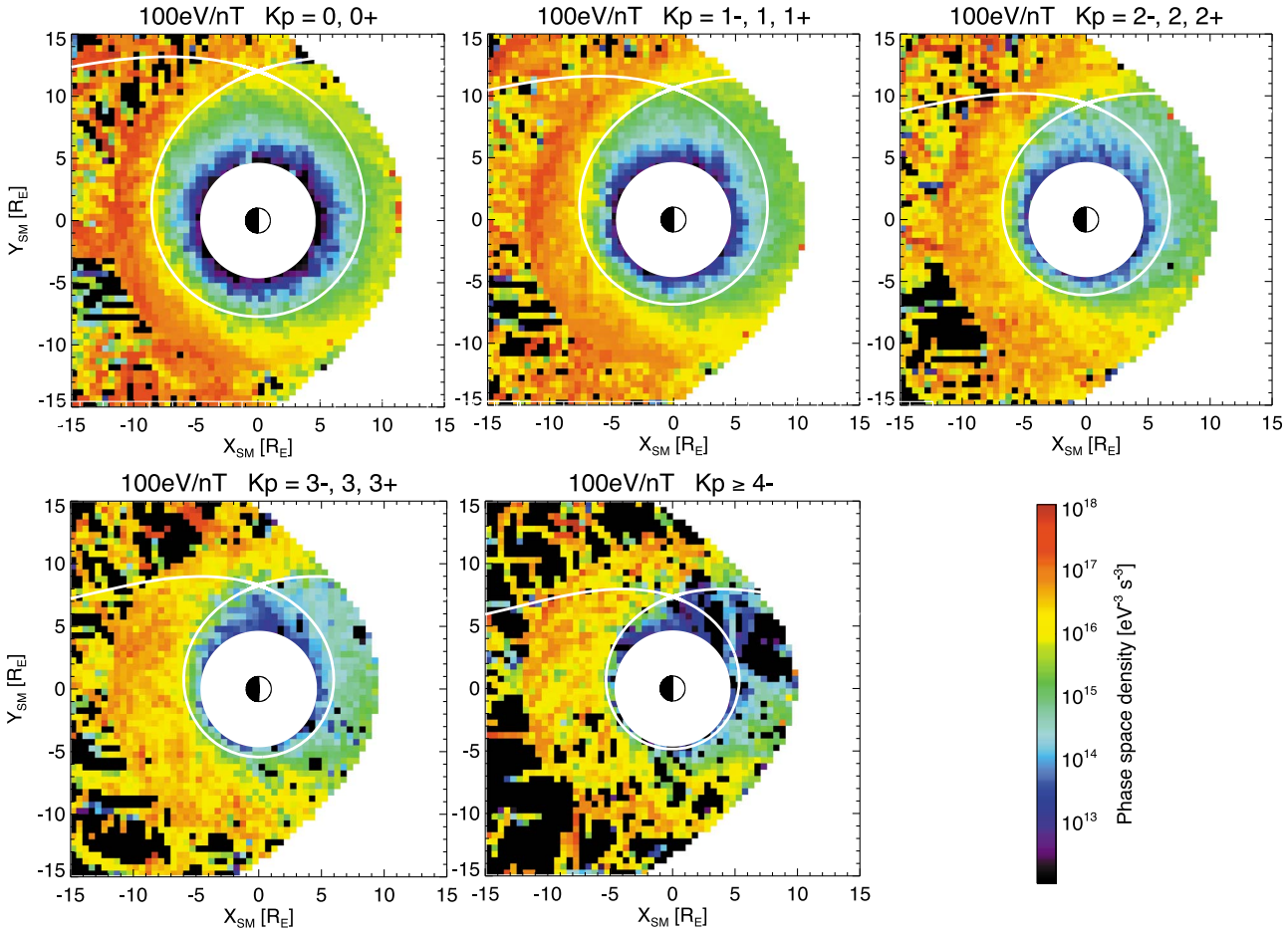

Figure 4. Same as Figure 3 but for electrons with 100 eV/nT.

culated Alfvén boundary for 100 eV/nT electrons are about 1 R_E further out than those for 50 eV/nT electrons for all *Kp* in Figure 4. Since the azimuthal drift component originating from gradient/curvature drifts depends on electron energies, the inner boundary of higher-energy (higher μ) electrons is further from the Earth than that of lower-energy (lower μ) electrons is.

[18] In Figures 3 and 4, we can see the good agreements between the observed and calculated boundary positions. These features are seen for all of the first adiabatic invariants we analyzed and it is confirmed that the boundary positions have μ dependence. These results are consistent with the particle drift paradigm.

3.2. Estimation of the Loss Time Scales From the Electron Data

[19] The PSD in the dawn and dayside sectors deceases along the electron drift path, suggesting losses of electrons by some wave-particle interactions [e.g., *Thomsen et al.*, 1998]. In this section, we quantitatively estimate electron loss time scales for μ = 50 and 100 eV/nT along the drift paths from the THEMIS observations.

[20] To estimate the electron loss time scales from the THEMIS observations, we derive the PSD distributions as a function of MLT along the drift paths. The drift paths of 50 and 100 eV/nT which pass 6 R_E at 6 MLT are shown in Figures 5a and 5b, respectively. The PSD of electrons with 50 eV/nT electrons for *Kp* = 1− to 1+ and 100 eV/nT electrons for *Kp* = 2− to 2+ along the drift paths are shown in Figures 5c and 5d, respectively. In Figures 5c and 5d, the exponential decay of the PSD is seen from the postmidnight sector to the dayside. The red lines in Figures 5c and 5d are the regression lines fitted by the least squares method for 2.1 to 10.2 MLT. To convert the slope of the regression line to the electron loss time scale τ, we calculate the *e*-folding azimuthal width $\Delta\varphi$ for the PSD decrease, and estimate the electron loss time scales from the time that the electron drift from 2.1 to 2.1 + $\Delta\varphi$ MLT. The Volland-Stern electric field and dipole magnetic field models are also used for calculating the drift times.

[21] The derived loss time scales are plotted as a function of the *Kp* index, which is shown in Figure 6 with black lines. The loss time scales for 50 and 100 eV/nT in *Kp* = 0 are ~4.2 and ~3.7 h, respectively. In *Kp* = 4, the loss time scales become significantly short, and those for 50 and 100 eV/nT are ~1.2 and ~0.56 h, respectively. The *Kp* dependence of the electron loss time scales implies that the enhancement of the loss during the magnetically disturbed period. We investigate

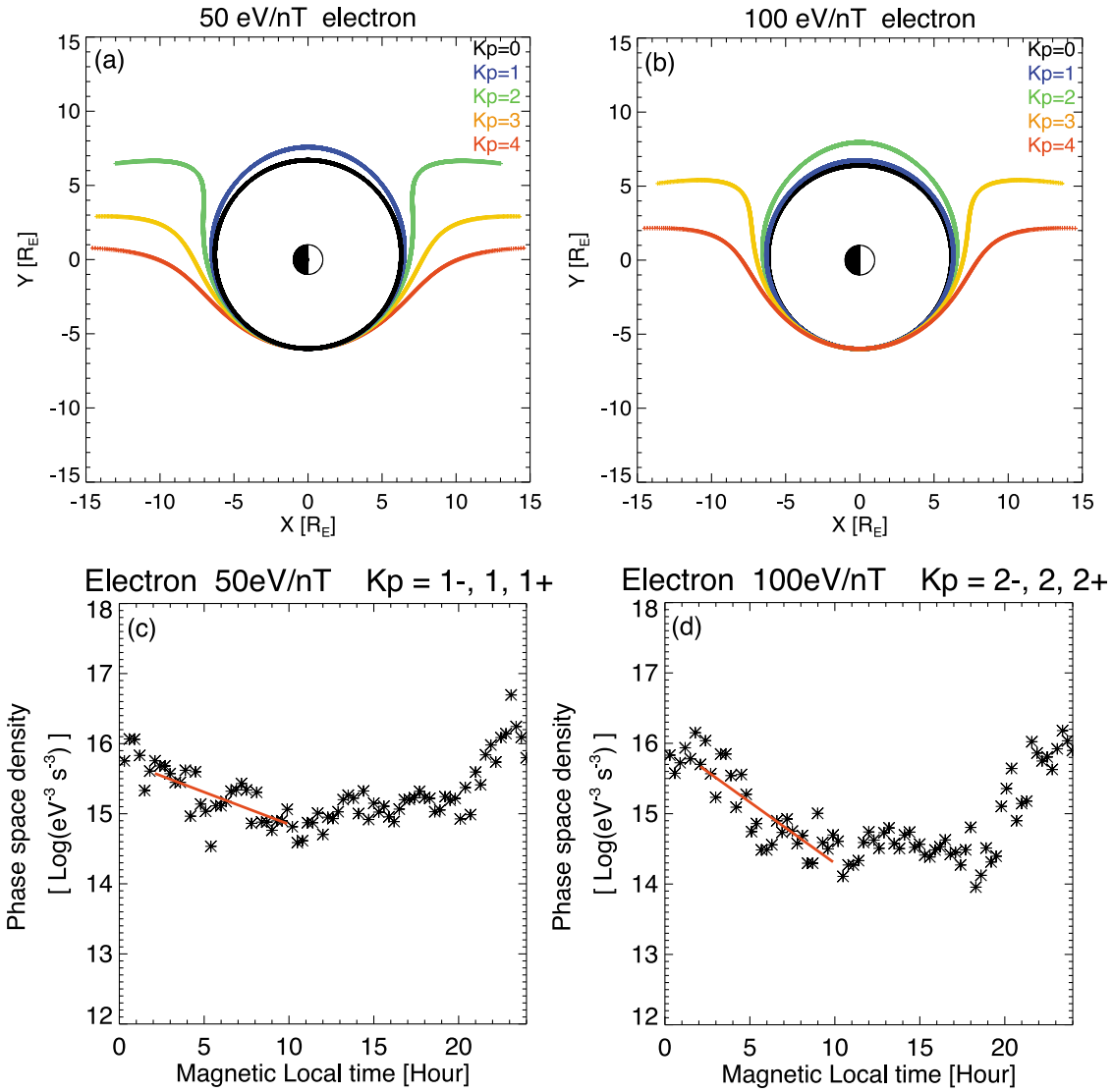

Figure 5. The drift paths of (a) 50 eV/nT and (b) 100 eV/nT electrons which pass $6R_E$ at 6 MLT. The drift paths are used for the estimation of the loss time scales based on the THEMIS observations. The MLT distribution of the PSD along the drift paths with (c) 50 eV/nT and (d) 100 eV/nT. Red lines represent the regression lines fitted by the least squares method from 2.1 MLT to 10.2 MLT.

possible loss processes from the point of view of wave-particle interactions in section 4.

4. Evaluation of Theoretical Loss Time Scales Based on Pitch Angle Diffusion Rate

[22] It has been suggested that whistler mode chorus waves outside the plasmasphere have sufficient power to cause strong diffusion [*Ni et al.*, 2008], compared with ECH waves [*Horne and Thorne*, 2000; *Horne et al.*, 2003a]. The chorus waves are frequently observed from the nightside through dawn to the dayside equatorial magnetosphere [e.g., *Meredith et al.*, 2001; *Li et al.*, 2009]. Therefore, the chorus wave is a primary candidate that interacts with plasma sheet electrons in the morning sector and causes them to precipitate into the atmosphere. In this section, we focus on the chorus wave-particle interactions as a possible source of the electron precipitation.

[23] To compare the loss time scales obtained from the THEMIS observations with theoretical loss time scales, we evaluate the decay rates τ_* due to the chorus waves along the drift paths using the approximated formula of *Albert and Shprits* [2009] with the quasi-linear pitch angle diffusion coefficients [*Albert*, 1999]. The expression of the decay rate τ_* [*Albert and Shprits*, 2009] is:

$$\tau_* = \int_{\alpha_L}^{\frac{\pi}{2}} \frac{1}{2D_{\alpha\alpha}(\alpha)\tan\alpha} \mathrm{d}\alpha, \quad [\mathrm{s}] \tag{6}$$

where $D_{\alpha\alpha}(\alpha)$ is the bounce-averaged pitch angle diffusion coefficient, and α_L is the loss cone angle. The wave parameters for the upper band and lower band chorus are the

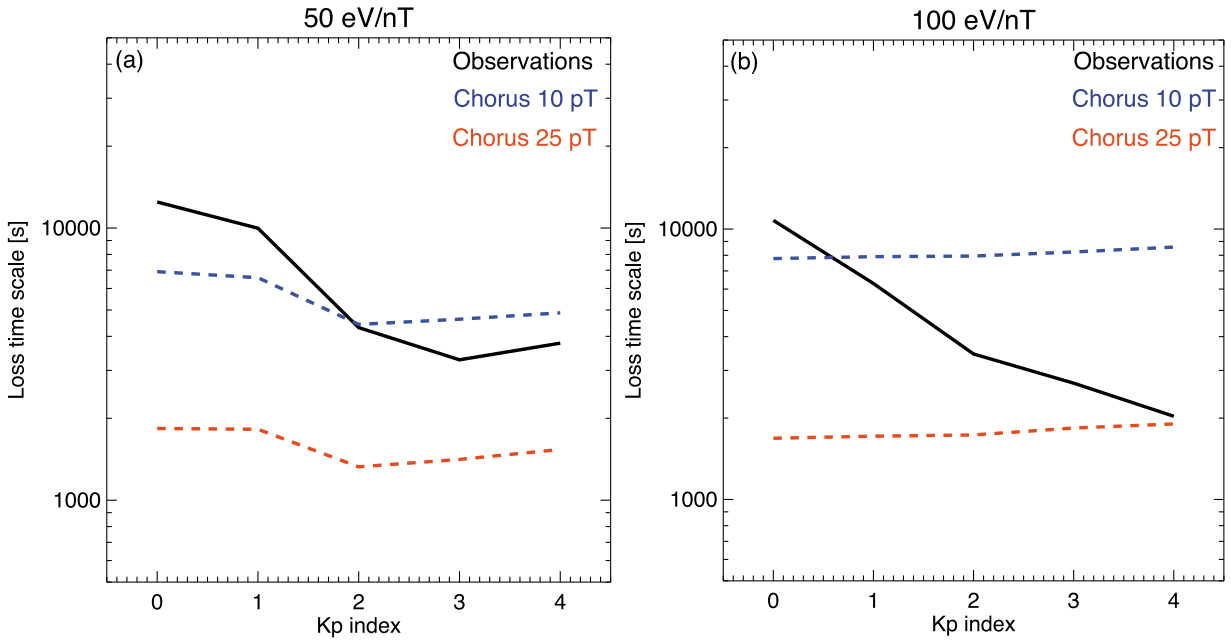

Figure 6. Black line indicates the loss time scales for (a) 50 eV/nT and (b) 100 eV/nT, evaluated from the THEMIS observations (see text). Dotted lines are the theoretical loss time scales due to the scattering by chorus waves with different amplitudes.

same as *Ni et al.* [2008] and *Horne et al.* [2003b], respectively. The wave amplitudes of the lower band chorus used in the calculations are 10 and 25 pT, and the same wave amplitudes are used for the upper band chorus. These wave amplitudes are based on the CRRES wave observations. The wave amplitude of 10 pT is comparable to an observed chorus amplitude during substorms [*Meredith et al.*, 2000] and that of 25 pT is a typical nightside chorus during the storm recovery phase [*Li et al.*, 2007]. We use the empirical plasmaspheric trough density model given by *Sheeley et al.* [2001] as the ambient density model. The calculation of the theoretical loss time scales is performed every 0.3 h MLT between 2.1 and 10.2 MLT, and we estimate the decay rates due to the pitch angle scattering by the chorus waves as the combination of the decay rates by the lower band and upper band chorus. In the calculations of the diffusion coefficients, we assume that the chorus wave amplitude is constant along the drift path. The plasma density and ambient magnetic field intensity for the calculation are evaluated at each position along the drift path using the *Sheeley et al.* [2001] density model and dipole field. To obtain the total loss time scales τ, we include the effect of the strong diffusion limit, and the expression by *Chen and Schulz* [2001] is used in the present study. Thus, the electron loss time scale is given as

$$\tau = \frac{\tau_* D_{SD} + 1}{D_{SD}}, \quad [\mathrm{s}] \tag{7}$$

where D_{SD} is the strong diffusion limit given by *Summers and Thorne* [2003].

[24] For the comparison of the observed loss time scales with the theoretical loss time scales, we average the theoretical loss time scales between 2.1 and 10.2 MLT along the drift paths. After the continuous loss along the drift path is accounted for, the PSD at 10.2 MLT ($f_{10.2\mathrm{MLT}}$) can be given by

$$f_{10.2\mathrm{MLT}} = f_{2.1\mathrm{MLT}} \prod_{i=2.1\mathrm{MLT}}^{10.2\mathrm{MLT}} e^{-\frac{\Delta t_i}{\tau_i}}, \tag{8}$$

where $f_{2.1\mathrm{MLT}}$ is the PSD at 2.1 MLT, Δt_i is the time that electrons spend the ith region, and τ_i is the theoretical loss time scale in region i. The PSD at 10.2 MLT can be expressed using the averaged theoretical loss time scale τ_{avg} as

$$f_{10.2\mathrm{MLT}} = f_{2.1\mathrm{MLT}}\, e^{-\frac{T}{\tau_{\mathrm{avg}}}}, \tag{9}$$

where T is the drift time from 2.1 to 10.2 MLT. Using equations (8) and (9), the averaged theoretical loss time scale is described as

$$\tau_{\mathrm{avg}} = -\frac{T}{\ln\left[\prod_i e^{-\frac{\Delta t_i}{\tau_i}}\right]} = \frac{T}{\sum_i \frac{\Delta t_i}{\tau_i}}. \tag{10}$$

We calculate the averaged theoretical loss time scales using equation (10), and the observed and theoretical loss time scales are plotted as a function of the *Kp* index in Figure 6 with dashed lines.

[25] The theoretical loss time scales at 10 pT roughly agree with the observed loss time scales at 50 eV/nT electrons for all *Kp* values, while there are discrepancies between the observed loss time scales at 100 eV/nT electrons for *Kp* = 3 and 4 and the theoretical loss time scales. This indicates that the wave amplitudes for *Kp* = 3 and 4 should be larger than 10 pT. The comparison of the observed loss time scales with the theoretical loss time scales at 25 pT shows that the loss time scales due to the chorus waves are small enough to explain the observed loss

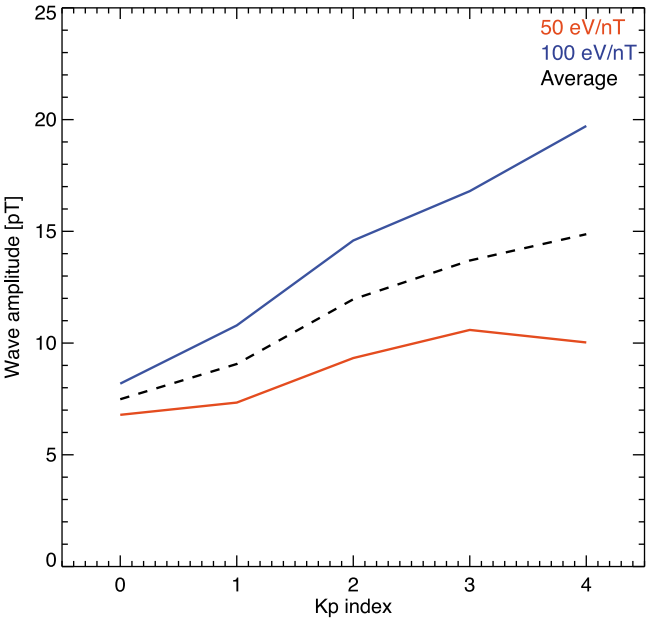

Figure 7. Required wave amplitudes of chorus waves that can explain the observed electron loss time scales as a function of the *Kp* index. The black dashed line indicates the average values of the required wave amplitudes with 50 (red line) and 100 eV/nT (blue line) electrons.

time scales. These comparisons suggest that plasma sheet electrons are scattered into the atmosphere significantly by the chorus waves.

5. Discussion

5.1. Electron Transport From the Plasma Sheet Into the Inner Magnetosphere

[26] Our analyses showed that the observed inner edge of the electron plasma sheet agreed with the calculated Alfvén boundary, which was consistent with the previous work by *Korth et al.* [1999]. Since our statistical analyses are based on a sufficient number of samples in the inner magnetosphere with wide radial distance coverage, the results are extended significantly from those obtained by *Korth et al.* [1999]. The present results confirm that electrons in the energy range of our analysis are a good tracer for the global convection electric field strength and that the averaged magnetic and global electric fields in the inner magnetosphere can be well described by the dipole magnetic field and Volland-Stern electric field models in a statistical sense.

[27] Since the theoretical Alfvén boundaries depend on the magnetic and electric field models, our analysis of the inner edge of the electron plasma sheet can be used for a direct test of the models. Assuming that the magnetic field of the inner magnetosphere is relatively well described by the dipole magnetic field, the analysis provides how accurately electric fields are estimated. *Korth and Thomsen* [2001] numerically conducted examinations based on the LANL MPA data on whether nonanalytic, semiempirical magnetic and electric field models can reproduce the observed Alfvén boundaries more accurately than the Volland-Stern and dipole magnetic field models can. Their results showed that more sophisticated numerical models do not always provide a better representation of the observed Alfvén boundaries than the combination of the Volland-Stern electric field and dipole magnetic field models do. Our statistical analysis showed that the Volland-Stern electric field model with the empirical potential model of *Maynard and Chen* [1975] can well describe distributions of electrons in the inner magnetosphere in a statistical sense, which is consistent with the conclusion of *Korth and Thomsen* [2001].

5.2. Electron Loss Time Scale

[28] The electron loss time scales in the morning sector was estimated to investigate electron loss mechanisms quantitatively. The observed electron loss time scales are almost consistent with the loss time scale due to the pitch angle scattering by chorus waves. Using the statistical results, it is possible to estimate appropriate wave amplitudes at each *Kp* value, instead of the wave amplitudes based on the observations as used in section 4. Considering that the theoretical loss time scale τ_* is proportional to the wave power, we estimated the required wave amplitudes at each *Kp* value by comparing τ_* with the loss time scales based on the electron measurements. The required wave amplitudes of chorus waves for 50and 100 eV/nT electrons are shown in Figure 7. There are discrepancies of the required wave amplitudes between 50 and 100 eV/nT (less than a factor of 2), and some of these discrepancies are due to the ambiguity of the assumed wave normal angle and the plasma parameters. The mean value of the required wave amplitudes at 50 and 100 eV/nT electrons are 7.48, 9.06, 12.0, 13.7, and 14.9 pT for Kp = 0, 1, 2, 3, and 4, respectively, while the observed average wave amplitudes of the chorus waves are a few pT during quiet conditions and enhanced during active conditions with amplitudes of $\gtrsim$ 10 pT [*Meredith et al.*, 2001]. Therefore, the required wave amplitudes are roughly consistent with the observed average amplitudes of the chorus waves. A comparison with the wave data obtained from the THEMIS satellites will be a future subject.

[29] As mentioned above, the observed electron loss time scales are shown to be consistent with the loss time scale due to the pitch angle scattering by chorus waves, and the required wave amplitudes are roughly consistent with previous statistical survey of chorus wave amplitudes. These investigations suggest that whistler mode chorus waves may be responsible for the loss of the plasma sheet electrons in the morning sector. The scattered electrons precipitate into the atmosphere, and contribute to diffuse auroral emissions in the morning sector [*Thomsen et al.*, 1998; *Chen and Schulz*, 2001; *Newell et al.*, 2009].

[30] ECH waves are another possible driver to cause diffuse auroral precipitations. By using the wave and particle data obtained from the CRRES satellite, *Meredith et al.* [1999] inferred that both ECH and whistler mode waves play significant roles in scattering the plasma sheet electrons to produce the diffuse aurora (whistler mode waves at $L \geq 6$ and ECH waves at $L \leq 6$, especially near the plasmapause). *Sergienko et al.* [2008] investigated the fine structure of the diffuse aurora using the high-sensitivity ground-based imager and the FAST electron measurements. They concluded that the strong pitch angle diffusion driven by ECH waves is responsible for the background diffuse aurora,

while the fine structure of the diffuse aurora is created by the precipitation of electrons with energies above 3–4 keV as a result of the pitch angle diffusion by the whistler mode waves. Further estimation of the drivers for precipitation of the diffuse aurora is necessary in future studies.

6. Summary

[31] Using the global electron distribution derived from large amount data obtained by the THEMIS satellites, we investigated the transport and loss of plasma sheet electrons in the inner magnetosphere. We showed a reasonable agreement between the observed inner boundaries of the electron plasma sheet and the calculated Alfvén boundaries. Our results reconfirmed that the transport of electrons from the magnetotail to the inner magnetosphere is controlled by large-scale dawn-dusk electric field. To investigate loss mechanisms of plasma sheet electrons in the morning side quantitatively, we derived the electron loss time scales from the average electron PSD distributions. The loss time scales based on the PSD distributions were compared with the theoretical ones due to the pitch angle scattering by chorus waves, by using the empirical wave models. The comparison revealed that the whistler mode chorus waves may contribute to the loss of the plasma sheet electrons in the morning sector. Furthermore, the required wave amplitudes inferred from the observed loss time scales roughly agreed with the previous statistical surveys of the chorus wave amplitudes. These suggest that the loss of plasma sheet electrons in the morning sector is mainly controlled by the whistler mode chorus waves, and the scattered electrons contribute to the generation of diffuse auroras in the morning sector.

[32] **Acknowledgments.** The authors would like to acknowledge NASA contract NAS5-02099 and the German Ministry for Economy and Technology and the German Center for Aviation and Space (DLR) under contract 50 OC 0302. The *Kp* index is provided by WDC for Geomagnetism, Kyoto. This research was supported by a special fund for education and research provided by the Ministry of Education, Culture, Sports, Science and Technology of Japan (MEXT) and the Support Program for Improving Graduate School Education from MEXT.

[33] Masaki Fujimoto thanks the reviewers for their assistance in evaluating this paper.

References

Albert, J. M. (1999), Analysis of quasi-linear diffusion coefficients, *J. Geophys. Res.*, *104*(A2), 2429–2411.

Albert, J. M., and Y. Y. Shprits (2009), Estimates of lifetimes against pitch angle diffusion, *J. Atmos. Sol. Terr. Phys.*, *71*, 1647–1552.

Angelopoulos, V. (2008), The THEMIS mission, *Space Sci. Rev.*, *141*(1–4), 5–34, doi:10.1007/s11214-008-9336-1.

Auster, H. U., et al. (2008), The THEMIS fluxgate magnetometer, *Space Sci. Rev.*, *141*(1–4), 235–264, doi:10.1007/s11214-008-9365-9.

Belmont, G., D. Fontaine, and P. Canu (1983), Are equatorial electron cyclotron waves responsible for diffuse auroral electron precipitation?, *J. Geophys. Res.*, *88*(A11), 9163–9170.

Birn, J., M. F. Thomsen, J. E. Borovsky, G. D. Reeves, D. J. McComas, and R. D. Belian (1997), Substorm ion injections: Geosynchronous observations and test particle orbits in three dimensional dynamic MHD fields, *J. Geophys. Res.*, *102*(A2), 2325–2341.

Chen, M. W., and M. Schulz (2001), Simulations of diffuse aurora with plasma sheet electrons in pitch angle diffusion less than everywhere strong, *J. Geophys. Res.*, *106*(A12), 28,949–28,966.

Ebihara, Y., M. Ejiri, H. Nilsson, I. Sandahl, A. Milillo, M. Grande, J. F. Fennell, and J. L. Roeder (2002), Statistical distribution of the storm-time proton ring current: POLAR measurements, *Geophys. Res. Lett.*, *29*(20), 1969, doi:10.1029/2002GL015430.

Fontaine, D., and M. Blanc (1983), A theoretical approach to the morphology and dynamics of diffuse auroral zones, *J. Geophys. Res.*, *88*(A9), 7171–7184.

Friedel, R. H. W., H. Korth, M. G. Henderson, M. F. Thomsen, and J. D. Scudder (2001), Plasma sheet access to the inner magnetosphere, *J. Geophys. Res.*, *106*(A4), 5845–5858.

Horne, R. B., and R. M. Thorne (2000), Electron pitch angle diffusion by electrostatic electron harmonic waves: The origin of pancake distributions, *J. Geophys. Res.*, *105*(A3), 5391–5402.

Horne, R. B., R. M. Thorne, N. P. Meredith, and R. R. Anderson (2003a), Diffuse auroral electron scattering by electron cyclotron harmonic and whistler mode waves during an isolated substorm, *J. Geophys. Res.*, *108*(A7), 1290, doi:10.1029/2002JA009736.

Horne, R. B., S. A. Glauert, and R. M. Thorne (2003b), Resonant diffusion of radiation belt electrons by whistler-mode chorus, *Geophys. Res. Lett.*, *30*(9), 1493, doi:10.1029/2003GL016963.

Jordanova, V. K., C. J. Farrugia, L. Janoo, J. M. Quinn, R. B. Torbert, K. W. Ogilvie, R. P. Lepping, J. T. Steinberg, D. J. McComas, and R. D. Belian (1998), October 1995 magnetic cloud and accompanying storm activity: Ring current evolution, *J. Geophys. Res.*, *103*(A1), 79–92.

Jordanova, V. K., Y. S. Miyoshi, S. Zaharia, M. F. Thomsen, G. D. Reeves, D. S. Evans, C. G. Mouikis, and J. F. Fennell (2006), Kinetic simulations of ring current evolution during the Geospace Environment Modeling challenge events, *J. Geophys. Res.*, *111*, A11S10, doi:10.1029/2006JA011644.

Kennel, C. F., F. L. Scarf, R. W. Fredricks, J. H. McGehee, and F. V. Coroniti (1970), VLF electric field observations in the magnetosphere, *J. Geophys. Res.*, *75*(31), 6136–6152.

Kerns, K. J., D. A. Hardy, and M. S. Gussenhoven (1994), Modeling of convection boundaries seen by CRRES in 120-eV to 28-keV particles, *J. Geophys. Res.*, *99*(A2), 2403–2414.

Korth, H., and M. F. Thomsen (2001), Plasma sheet access to geosynchronous orbit: Generalization to numerical global field models, *J. Geophys. Res.*, *106*(A12), 29,655–29,667.

Korth, H., M. F. Thomsen, J. E. Borovsky, and D. J. McComas (1999), Plasma sheet access to geosynchronous orbit, *J. Geophys. Res.*, *104*(A11), 25,047–25,062.

Li, W., Y. Y. Shprits, and R. M. Thorne (2007), Dynamic evolution of energetic outer zone electrons due to wave-particle interactions during storms, *J. Geophys. Res.*, *112*, A10220, doi:10.1029/2007JA012368.

Li, W., R. M. Thorne, V. Angelopoulos, J. Bortnik, C. M. Cully, B. Ni, O. Le Contel, A. Roux, U. Auster, and W. Magnes (2009), Global distribution of whistler-mode chorus waves observed on the THEMIS spacecraft, *Geophys. Res. Lett.*, *36*, L09104, doi:10.1029/2009GL037595.

Li, W., et al. (2010), THEMIS analysis of observed equatorial electron distributions responsible for the chorus excitation, *J. Geophys. Res.*, *115*, A00F11, doi:10.1029/2009JA014845.

Lui, A. T. Y., D. Venkatesan, C. D. Anger, S. I. Akasofu, W. J. Heikkila, J. D. Winningham, and J. R. Burrows (1977), Simultaneous observations of particle precipitations and auroral emissions by the Isis 2 satellite in the 1900–2400 MLT sector, *J. Geophys. Res.*, *82*(16), 2210–2226.

Lyons, L. R. (1974), Electron diffusion driven by magnetospheric electrostatic waves, *J. Geophys. Res.*, *79*(4), 575–580.

Lyons, L. R., R. M. Thorne, and C. F. Kennel (1972), Pitch-angle diffusion of radiation belt electrons within the plasmasphere, *J. Geophys. Res.*, *77*(19), 3455–3474.

Maynard, N. C., and A. J. Chen (1975), Isolated cold plasma regions: Observations and their relation to possible production mechanisms, *J. Geophys. Res.*, *80*(7), 1009–1013.

McFadden, J. P., C. W. Carlson, D. Larson, V. Angelopoulos, M. Ludlam, R. Abiad, B. Elliott, P. Turin, and M. Marckwordt (2008a), The THEMIS ESA plasma instrument and in-flight calibration, *Space Sci. Rev.*, *141*(1–4), 277–302, doi:10.1107/s11214-008-9440-2.

McFadden, J. P., C. W. Carlson, D. Larson, J. Bonnell, F. Mozer, V. Angelopoulos, K.-H. Glassmeier, and U. Auster (2008b), THEMIS ESA first science results and performance issues, *Space Sci. Rev.*, *141*(1–4), 477–508, doi:10.1007/s11214-008-9433-1.

Meng, C.-I., B. Mauk, and C. E. McIlwain (1979), Electron precipitation of evening difuse aurora and its conjugate electron fluxes near the magnetospheric equator, *J. Geophys. Res.*, *84*(A6), 2545–2558.

Meredith, N. P., A. D. Johnstone, S. Szita, R. B. Horne, and R. R. Anderson (1999), "Pancake" electron distributions in the outer radiation belts, *J. Geophys. Res.*, *104*(A6), 12,431–12,444.

Meredith, N. P., R. B. Horne, A. D. Johnstone, and R. R. Anderson (2000), The temporal evolution of electron distributions and associated wave activity following substorm injections in the inner magnetosphere, *J. Geophys. Res.*, *105*(A6), 12,907–12,917.

Meredith, N. P., R. B. Horne, and R. R. Anderson (2001), Substorm dependence of chorus amplitudes: Implications for the acceleration of electrons to relativistic energies, *J. Geophys. Res.*, *106*(A7), 13,165–13,178.

Meredith, N. P., R. B. Horne, S. A. Glauert, D. N. Baker, S. G. Kanekal, and J. M. Albert (2009), Relativistic electron loss time scales in the slot region, *J. Geophys. Res.*, *114*, A03222, doi:10.1029/2008JA013889.

Miyoshi, Y., A. Morioka, T. Obara, H. Misawa, T. Nagai, and Y. Kasahara (2003), Rebuilding process of the outer radiation belt during the 3 November 1993 magnetic storm: NOAA and Exos-D observations, *J. Geophys. Res.*, *108*(A1), 1004, doi:10.1029/2001JA007542.

Miyoshi, Y., A. Morioka, R. Kataoka, Y. Kasahara, and T. Mukai (2007), Evolution of the outer radiation belt during the November 1993 storms driven by corotating interaction regions, *J. Geophys. Res.*, *112*, A05210, doi:10.1029/2006JA012148.

Newell, P. T., T. Sotirelis, and S. Wing (2009), Diffuse, monoenergetic, and broadband aurora: The global precipitation budget, *J. Geophys. Res.*, *114*, A09207, doi:10.1029/2009JA014326.

Ni, B., R. M. Thorne, Y. Y. Shprits, and J. Bortnik (2008), Resonant scattering of plasma sheet electrons by whistler-mode chorus: Contribution to diffuse auroral precipitation, *Geophys. Res. Lett.*, *35*, L11106, doi:10.1029/2008GL034032.

Roeder, J. L., and H. C. Koons (1989), A survey of electron cyclotron waves in the magnetosphere and the diffuse auroral precipitation, *J. Geophys. Res.*, *94*(A3), 2529–2541.

Sergienko, T., I. Sandahl, B. Gustavsson, L. Andersson, U. Brändström, and Å. Steen (2008), A study of fine structure of diffuse aurora with ALIS-FAST measurements, *Ann. Geophys.*, *26*, 3185–3195.

Sheeley, B. W., M. B. Moldwin, H. K. Rassoul, and R. R. Anderson (2001), An empirical plasmasphere and trough density model: CRRES observations, *J. Geophys. Res.*, *106*(A11), 25,631–25,641.

Stern, D. P. (1975), Motion of a proton in the equatorial megentosphere, *J. Geophys. Res.*, *80*(4), 595–599.

Summers, D., and R. M. Thorne (2003), Relativistic electron pitch-angle scattering by electromagnetic ion cyclotron waves during geomagnetic storms, *J. Geophys. Res.*, *108*(A4), 1143, doi:10.1029/2002JA009489.

Thomsen, M. F., D. J. McComas, J. E. Borovsky, and R. C. Elphic (1998), The magnetospheric trough, in *Geospace Mass and Energy Flow: Results From the International Solar-Terrestrial Physics Program*, *Geophys. Monogr. Ser.*, vol. 104, edited by J. L. Horwitz et al., pp. 355–369, AGU, Washington, D. C.

Tsyganenko, N. A. (1989), A magnetospheric magnetic field model with a warped tail current sheet, *Planet. Space Sci.*, *37*, 5–20.

Volland, H. A. (1973), A semiempirical model of large scale magnetospheric electric fields, *J. Geophys. Res.*, *78*, 171–180.

Wang, C.-P., L. R. Lyons, V. Angelopoulos, D. Larson, J. P. McFadden, S. Frey, H. Auster, and W. Magnes (2008), THEMIS observations of penetration of the plasma sheet into the ring current region during a magnetic storm, *Geophys. Res. Lett.*, *35*, L17S14, doi:10.1029/2008GL033375.

Whipple, E. C., Jr. (1978), (*U*, *B*, *K*) coordinates: A natural system for studying magnetospheric convection, *J. Geophys. Res.*, *83*(A9), 4318–4326.

Yao, Y., K. Seki, Y. Miyoshi, J. P. McFadden, E. J. Lund, and C. W. Carlson (2008), Effect of solar wind variation on low-energy O+ populations in the magnetosphere during geomagnetic storms: FAST observations, *J. Geophys. Res.*, *113*, A04220, doi:10.1029/2007JA012681.

J. M. Albert, Space Vehicles Directorate, Air Force Research Laboratory, 29 Randolph Rd., Hanscom Air Force Base, MA 01731-3010, USA.

V. Angelopoulos, Institute of Geophysics and Planetary Physics, University of California, Los Angeles, CA 90095-1567, USA.

H. U. Auster, Institut für Geophysik und Extraterrestrische Physik, Technische Universität Braunschweig, Mendelssohnstr. 3, D-38106 Braunschweig, Germany.

T. Hori, Y. Miyashita, Y. Miyoshi, and Y. Nishimura, Solar-Terrestrial Environment Laboratory, Furo-cho, Chikusa-ku, Nagoya 464-8601, Japan.

V. Jordanova, Los Alamos National Laboratory, Los Alamos, NM 87545, USA.

S. Kurita, H. Misawa, A. Morioka, and F. Tsuchiya, Planetary Plasma and Atmospheric Research Center, Tohoku University, Aramaki-aza-aoba, Aoba, Sendai, Miyagi 980-8578, Japan. (kurita@pparc.gp.tohoku.ac.jp)

J. P. McFadden, Space Sciences Laboratory, University of California, Berkeley, CA 94720, USA.

T. Takada, Department of Electrical Engineering and Information Science, Kochi National College of Technology, 200-1 Monobe-otsu, Nankoku, Kochi 783-8508, Japan.